Formation Mechanism of AlN Inclusion in High-Nitrogen Stainless Bearing Steels

PENG-CHONG LU, HUA-BING LI, HAO FENG, ZHOU-HUA JIANG, HONG-CHUN ZHU, ZHUANG-ZHUANG LIU, and TONG HE

The existence of angular and hard AlN inclusions would seriously deteriorate the service life of high-nitrogen stainless bearing steels (HNSBSs). In this work, the formation mechanism of AlN inclusion in HNSBSs under as-cast, annealing and austenitizing states was systematically investigated by microstructure observation and thermodynamic, kinetic analyses. The results showed that the concentration product of Al and N could exceed the critical solubility of AlN inclusion at liquidus temperature with the Al content higher than 0.050 wt pct, which led to the formation of AlN inclusions about 1 to 5 μm (equivalent diameter) in liquid steel. Based on the 'Clyne-Kurz' model, AlN inclusion could form at the solidifying front due to the enrichment of N in the residual liquid steel with the Al content higher than 0.030 wt pct. Besides, the precipitation of Cr_2N and the extremely low diffusion coefficient of Al in α phase restrained the precipitation of AlN during annealing at 1023 K. However, AlN and AlN-MnS composite inclusions less than 0.6 μm could precipitate during austenitizing at 1323 K with the Al content higher than 0.006 wt pct, which was the critical Al content to avoid AlN formation in HNSBSs after melting, solidification, and heat treatment processes.

I. INTRODUCTION

THE beneficial effects of nitrogen (N) on mechanical properties and corrosion resistance of austenitic,[1–3] duplex,[4–6] and martensitic[7–9] stainless steels have been widely investigated. In particular, high-nitrogen martensitic stainless steels exhibit high hardness, high strength and toughness, excellent corrosion, and fatigue resistance, which are widely applied in aviation bearing and other fields.[7,10,11] The service life of bearings is largely determined by the cleanliness of the steel.[12–14] Specially, oxygen is a common impurity element in bearing steel, which could promote the formation of inclusions.[15–17] Accordingly, reducing oxygen content and improving the cleanliness of the steel are the key factors for the development of bearing steels.

It is well known that aluminum (Al) is a conventional and highly effective deoxidizer, while it is also a strong nitride-forming element.[18–20] For the high-nitrogen stainless bearing steel (HNSBS) alloy system, the high N content, such as 0.3 to 0.5 wt pct in Cronidur 30 (developed by Energietechnik Essen GmbH for rolling bearing and ball screw applications),[11] is easy to induce the formation of AlN inclusion. Thereafter, the internal cracks would be easily generated around the angular and hard AlN inclusion,[21] leading to bearing failure *via* rolling contact fatigue (RCF, a typical failure mode of rolling bearings and similar machine parts).[22] Wilson *et al.*[23] reported that AlN would also result in the embrittlement or cracking of rolled/forged products. Therefore, it is very necessary to investigate the formation mechanism of AlN inclusion and acquire the critical Al content to avoid AlN formation in HNSBSs.

In recent years, the thermodynamics and kinetics of AlN formation in high-Al steels have been widely reported, and the formation of AlN in liquid steel, during solidification and heat treatment processes, has been investigated.[18,24–32] Jang *et al.*[18] reported the formation of AlN in liquid high-Al, high-Mn alloyed steels and obtained the critical N content to avoid AlN formation. Besides, Croft *et al.*[24–26] indicated that the segregation of Al and N in the residual liquid steel during solidification process led to the formation of AlN inclusion at the solidifying front. Moreover, some researchers believed that AlN could precipitate during

PENG-CHONG LU, HAO FENG, HONG-CHUN ZHU, and ZHUANG-ZHUANG LIU are with the School of Metallurgy, Northeastern University, Shenyang, 110819, P.R. China. HUA-BING LI and ZHOU-HUA JIANG are with the School of Metallurgy, Northeastern University and also with the State Key Laboratory of Rolling and Automation, Northeastern University, Shenyang, 110819, P.R. China. contact e-mail: lihb@smm.neu.edu.cn TONG HE is with the Analysis and Testing Centre, Northeastern University, Shenyang, 110819, P.R. China.

either isothermal holding or continuous-cooling on passing through the $\gamma \rightarrow \alpha$ transformation region.[23,29,30,33] Nevertheless, up to now, the formation mechanism of AlN inclusion in high-N steels was rarely reported.

In view of the deleterious effect of AlN inclusion to the service life of bearing steel, HNSBSs with various Al contents were prepared using the pressurized metallurgy method. The formation processes of AlN inclusion under as-cast, annealing, and austenitizing states were systematically investigated. Furthermore, the thermodynamics and kinetics of AlN precipitation were analyzed to clarify the formation mechanism of AlN inclusion and obtain the critical Al content to avoid AlN formation in HNSBSs.

II. EXPERIMENTAL PROCEDURES AND ANALYSIS METHOD

A. Materials Preparation

The HNSBSs with various Al contents were smelted using a 25 kg pressurized induction furnace, and the compositions of the steels are listed in Table I. Subsequently, in order to investigate the formation processes of AlN inclusion in liquid steel, and during solidification, annealing, and austenitizing processes, several specimens under different states were prepared: (1) as-cast (from the center and edge of steel ingots), (2) annealing at 1023 K for 120 min followed by oil quenching, and (3) austenitizing at 1323 K for 120 min followed by oil quenching. It is worth noting that the HNSBSs were normally annealed at 1023 K to 1073 K, austenitized at 1293 K to 1323 K. The dimension of the ingot and the positions of the sampling specimens and thermocouple are shown in Figure 1. The thermocouple was used to measure the cooling rate of molten steel during solidification process.

B. Microstructure Characterization

The specimens used for microstructure observation were mechanically ground with silicon carbide papers to 2000-grit and polished with 2.5 μm diamond paste. Then the microstructure of the specimens was characterized using a field emission scanning electron microscope (FE-SEM, Carl Zeiss Ultra Plus) equipped with an energy-dispersive spectroscopy (EDS). For the austenitized specimens, twenty view fields were selected randomly to statistically analyze the number and size of AlN inclusion using Image-Pro Plus 6.0 software. The effective minimum size of the inclusions which could be detected by the image analysis software was 0.1 μm. Simultaneously, the precipitation type in 0.076Al steel was also characterized by a transmission electron microscope (TEM, FEI Tecnai G^2 20), and the thin disks for TEM observation were prepared on the basis of the previous work.[34]

The polished specimens used for measuring the dendrite arm spacing were etched with a mixed solution (1 g picric acid + 5 g FeCl$_3$ + 15 mL hydrochloric acid + 50 mL H$_2$O). The dendritic structure was observed using a digital microscope (Olympus DXS 510). Ten view fields were selected randomly to statistically analyze the secondary dendrite arm spacing via the OLYCIA m3 image analysis software.

C. Thermodynamic and Kinetic Analysis Method

1. Thermodynamics equation of AlN formation in liquid steel

The thermodynamics of AlN formation in liquid steel were analyzed by the reaction equilibrium equations, which can be described as follows:[25,26,35]
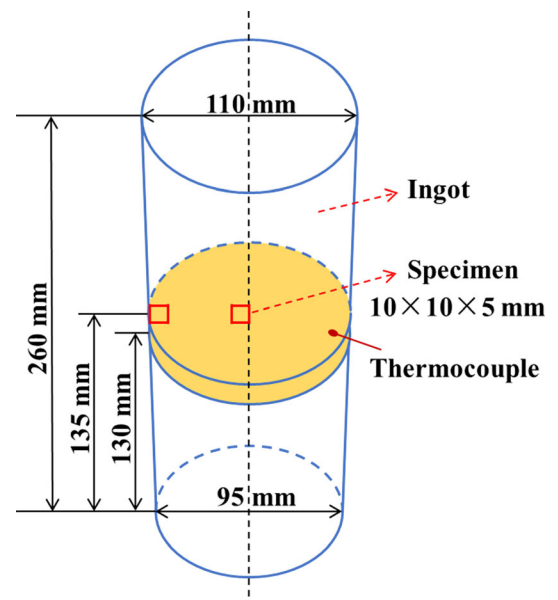

Fig. 1—The dimension of the ingot and the positions of the sampling specimens and thermocouple.

Table I. Chemical Compositions of High-Nitrogen Stainless Bearing Steels (Wt Pct)

Specimens	C	Cr	Mo	N	Mn	Si	S	O	Sol. Al	Fe
0.006Al	0.32	15.20	1.03	0.40	0.43	0.51	0.002	0.0019	0.006	bal.
0.008Al	0.31	15.18	1.04	0.41	0.42	0.50	0.002	0.0018	0.008	bal.
0.013Al	0.31	15.21	1.02	0.39	0.44	0.52	0.002	0.0015	0.013	bal.
0.026Al	0.32	15.23	1.03	0.37	0.43	0.53	0.003	0.0014	0.026	bal.
0.045Al	0.32	15.20	1.01	0.40	0.42	0.53	0.002	0.0013	0.045	bal.
0.076Al	0.32	15.15	1.02	0.45	0.45	0.52	0.002	0.0009	0.076	bal.

$$[Al] + [N] = (AlN)_{(s)}$$
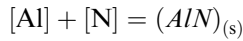
$$\Delta G_{AlN}^{\Theta} = -245990 + 107.59T \qquad [1]$$

where ΔG_{AlN}^{Θ} (J mol^{-1}) is the standard Gibbs free energy change. The activity of AlN is unity in the present study (pure solid as the standard state). In addition, the equilibrium constant K_{AlN} of reaction [1] is calculated as follows:

$$
\begin{aligned}
\log K_{AlN} = \log \frac{a_{AlN}}{a_{Al} \cdot a_N} &= \log a_{AlN} - \log a_{Al} - \log a_N \\
&= -\log(f_{Al} \cdot [\text{pct Al}]) \\
&\quad - \log(f_N \cdot [\text{pct N}])
\end{aligned}
\qquad [2]
$$

where f_{Al} and f_N are the activity coefficients of Al and N dissolved in liquid steel, respectively. [pct Al] and [pct N] are the mass percent of Al and N in liquid steel, respectively. The value of f_i is calculated as follows:

$$\log f_i = \Sigma(e_i^j \cdot [\text{pct } j] + r_i^j \cdot [\text{pct } j]^2) \qquad [3]$$

(i = Al, N; j = C, Cr, Mo, Mn, Si, S, P, O, N, Al)

The first-order interaction parameters (e_i^j) and the second-order interaction parameters (r_i^j) used in this study are listed in Tables II and III, respectively:

Accordingly, the critical solubility product K_{AlN}^{prime} of AlN formation (the product of [pct Al] and [pct N] when the reaction [1] reaches equilibrium) can be derived from Eqs. [1] through [3] as follows:

$$K_{AlN}^{prime} = [\text{pct Al}][\text{pct N}] \qquad [4]$$

When the actual product of [pct Al] and [pct N] in the liquid phase exceeded the value of K_{AlN}^{prime}, AlN inclusions would form in liquid steel.[26]

2. Thermodynamics Model of AlN Formation during Solidification Process

AlN inclusion could also form in the residual steel due to the segregation of Al and N during solidification process.[25,40] For this reason, different models, such as 'Lever-rule' model[26,41] and Scheils equation,[25,41] had been used to calculate the concentrations of Al and N in the residual liquid phase during solidification process depending on the degree of solute diffusion in the solid, respectively. However, 'Lever-rule' model assumes that all the solute elements mix completely in both the liquid and solid phases during solidification process, which is usually not valid due to the extremely low diffusion rate in the solid phases.[40] Besides, Scheils equation assumes that no diffusion in the solid phase occur, in which final concentration of the solute tends to infinity.[40] Accordingly, finite diffusion should be considered in the solid phase to predict the segregation during solidification process of the molten steel.

'Clyne-Kurz' model,[40,42,43] which considers the finite diffusion, is relatively closer to the real situation, as shown in Eq. [5]:

$$C_L = C_0[1 - (1 - 2\Omega k_i)f_S]^{\frac{(k_i-1)}{(1-2\Omega k_i)}} \qquad [5]$$

where C_L is the concentration of the solutes in the liquid phase at solid–liquid interface, C_0 is the initial liquid concentration, f_S is the solid fraction, and k_i is the equilibrium partition coefficient for the element i, defined as the ratio of solute composition in the solid (C_S) to that in the liquid (C_L) at equilibrium during solidification process[44]:

$$k_i = \frac{C_S}{C_L} \qquad [6]$$

Ω is a modified back-diffusion parameter, calculated as follows:

$$\Omega = \alpha\left[1 - \exp\left(-\frac{1}{\alpha}\right)\right] - \frac{1}{2}\exp\left(-\frac{1}{2\alpha}\right) \qquad [7]$$

where α is a back-diffusion parameter, which is defined as follows:

$$\alpha = \frac{D^S t_f}{(0.5\lambda_S)^2} \qquad [8]$$

where D^S (m^2 s^{-1}) is the diffusion coefficient of solute in the solid phase; λ_S is the secondary dendrite arm spacing; and t_f (s) is the local solidification time, defined as follows:

$$t_f = \frac{T_L - T_S}{C_R} \qquad [9]$$

where C_R (K s^{-1}) is the cooling rate. Therefore, the concentrations of Al and N in the residual liquid phase during solidification process could be expressed as follows:

Table III. The Second-Order Interaction Parameters Used in This Study

γ_i^j	C	Si	Al
Al	-0.004[36]	-0.0006[36]	$-0.0011 + 0.17/T$[36]
N	—	0.0012[36]	—

Table II. The First-Order Interaction Parameters Used in This Study

e_i^j	C	Cr	Mo	Mn	Si	S	P	O	N	Al
Al	0.091[36]	0.03[37]	—	0.035[37]	0.056[36]	0.035[25]	0.033[25]	-1.98[26]	$-627.1/T + 0.367$[38]	$0.011 + 63/T$[39]
N	0.13[26]	-0.046[25]	-0.011[25]	-0.02[38]	0.048[26]	0.007[25]	0.059[25]	—	—	0.01[25]

$$[\text{pct Al}] = [\text{pct Al}]_0[1 - (1 - 2\Omega k_{\text{Al}})f_{\text{S}}]^{\frac{(k_{\text{Al}}-1)}{(1-2\Omega k_{\text{Al}})}} \quad [10]$$

$$[\text{pct N}] = [\text{pct N}]_0[1 - (1 - 2\Omega k_{\text{N}})f_{\text{S}}]^{\frac{(k_{\text{N}}-1)}{(1-2\Omega k_{\text{N}})}} \quad [11]$$

where $[\text{pct Al}]_0$ and $[\text{pct N}]_0$ are the initial concentrations of Al and N in liquid steel, respectively; k_{Al} and k_{N} are the equilibrium partition coefficients of Al and N, respectively. When the product of $[\text{pct Al}]$ and $[\text{pct N}]$ (calculated by Eqs. [10] and [11]) exceeded the value of K_{AIN}^{prime}, AlN inclusions would form during solidification process.

3. Thermodynamic and Kinetic Analysis Method During Heat Treatment Processes

The thermodynamics and kinetics of AlN formation in HNSBSs during heat treatment processes were analyzed using Thermo-Calc and DICTRA software, respectively.

III. RESULTS AND DISCUSSION

A. AlN Formation in As-cast HNSBSs

Figure 2 shows the morphologies of inclusions in as-cast 0.076Al, 0.045Al, and 0.026Al ingots. AlN inclusions about 1.0 to 5.0 μm (equivalent diameter) and 0.5 to 1.0 μm emerged in 0.076Al ingot and 0.045Al ingot, respectively. However, no AlN inclusions were

detected in the other four experimental ingots, indicating that AlN inclusion could not form in liquid state or during solidification process in HNSBSs containing 0.026 wt pct or lower Al contents. Besides, a small amount of Al_2O_3 inclusions was found in 0.026Al ingot, as shown in Figures 2(e) and (f).

1. Thermodynamics Analysis of AlN Formation in Liquid Steel

The critical solubility product of AlN formation in liquid steel calculated *via* Eqs. [1] through [4] is shown as follows:

$$K_{AIN}^{prime} = [\text{pct Al}][\text{pct N}] = 10^{5.730-12849.169/T} \quad [12]$$

Accordingly, the stability diagram of AlN formation in HNSBSs is shown in Figure 3. The solid and dashed lines represent the critical solubility of AlN inclusion at liquidus (T_{L} = 1731 K) and solidus temperature (T_{S} = 1674 K), respectively, which were calculated using Thermo-Calc software. Points 1, 2, 3, 4, 5, and 6 represent the 0.076Al, 0.045Al, 0.026Al, 0.013Al, 0.008Al, and 0.006Al steels, respectively. It shows that point 1 is higher than the solid line, revealing that AlN inclusion could form in liquid 0.076Al steel, which is consistent with the morphology in Figure 2(a) and (b). However, points 2 to 6 are below the solid line, indicating that when the temperature was higher than the liquidus temperature, the thermodynamic conditions for AlN formation in 0.026Al, 0.013Al, 0.008Al, and 0.006Al steels could not be satisfied, i.e., AlN inclusion could not form in liquid steel.
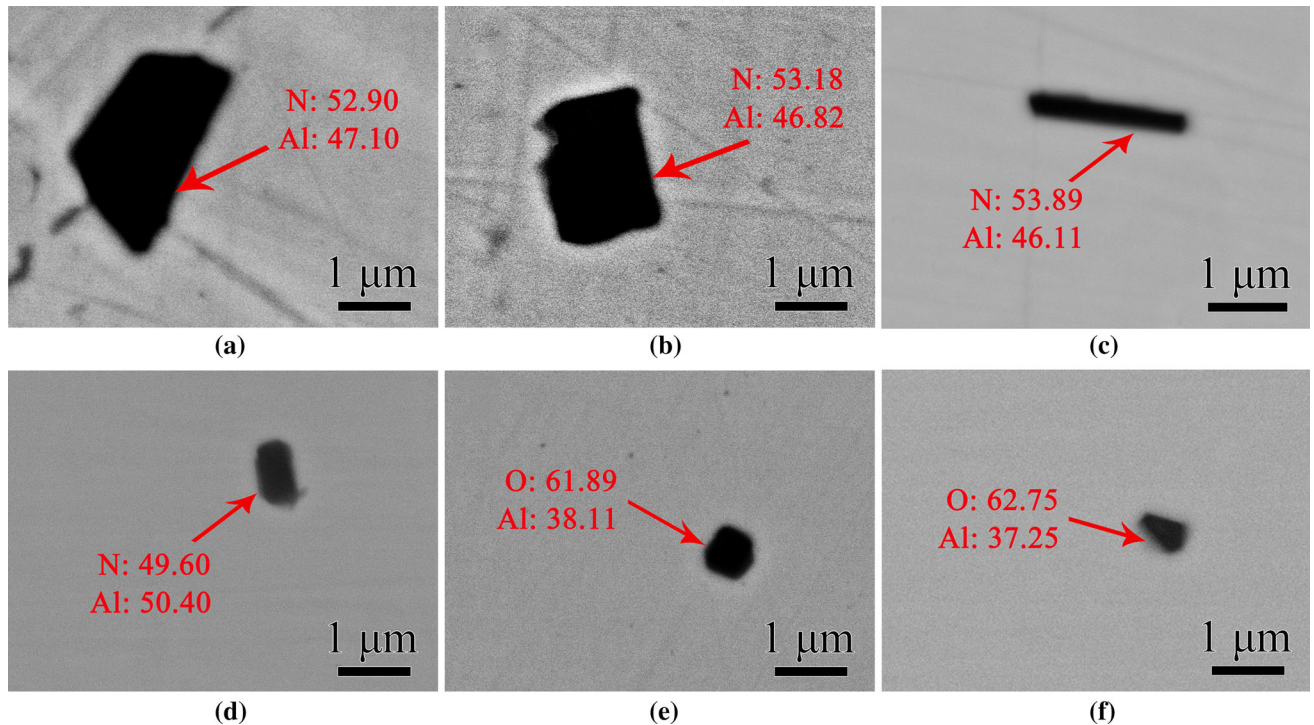

Fig. 2—The morphologies of inclusions in as-cast ingots: (*a*) 0.076Al-center; (*b*) 0.076Al-edge; (*c*) 0.045Al-center; (*d*) 0.045Al-edge; (*e*) 0.026Al-center; (*f*) 0.026Al-edge.

According to the critical solubility of AlN inclusion at liquidus temperature, the critical Al content of AlN inclusion formation in liquid steel is 0.050 wt pct when the N content is 0.4 wt pct. Therefore, in order to avoid the formation of AlN inclusion in liquid steel, the Al content in HNSBSs should be lower than 0.050 wt pct.

2. Thermodynamics Analysis of AlN Formation During Solidification Process

As shown in Figure 3, point 3 is between the solid line and the dashed line, indicating that AlN inclusion might form in 0.045Al steel during solidification process. Meanwhile, points 3 to 6 are below the dashed line, illustrating that the thermodynamic conditions for AlN formation in 0.026Al, 0.013Al, 0.008Al, and 0.006Al steels could not be satisfied during solidification process. Nevertheless, when the temperature of steels dropped below the liquidus temperature, the formation of AlN
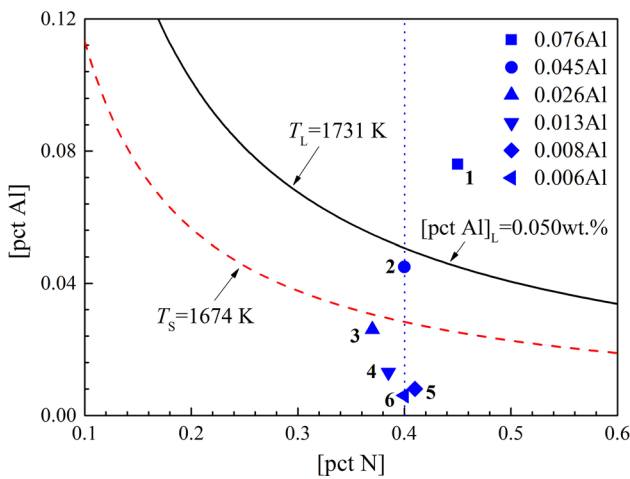

Fig. 3—The stability diagram of AlN formation in HNSBSs.

inclusion might occur at the solidifying front because of the segregation of Al and N in the residual liquid steel.[25,40] In view of the absence of AlN inclusion in as-cast ingots with the Al content lower than 0.026 wt pct, the concentrations of Al and N in the liquid phase at the solidifying front of 0.026Al steel ([pct Al] and [pct N]) were investigated.

According to the 'Clyne-Kurz' model, it could be seen that the segregation of element i is a function of secondary dendrite arm spacing (λ_S), cooling rate (C_R), equilibrium partition coefficient (k_i), and diffusion coefficient (D^S). The dendrite structure of the 0.026Al steel is shown in Figure 4. It is obvious that the secondary dendrite arm spacing (λ_S) at the ingot center is larger than that at the ingot edge significantly. The values of λ_S at the center and edge of 0.026Al ingot are about 4×10^{-5} and 2×10^{-5} m, respectively.

In addition, the cooling curve of the edge in experimental steel measured by the thermocouple is shown in Figure 5. It could be seen that the cooling rate (C_R) in the ingot edge during the solidification process is nearly uniform, about 3.8 K s^{-1}. According to the previous work by Zhu et al.,[45] the cooling rate at the ingot edge was approximately 5 times that at the ingot center. Hence, the cooling rate at the ingot center was about 0.8 K s^{-1}.

In order to obtain the equilibrium partition coefficients and diffusion coefficients of Al and N, the equilibrium phase and phase composition fractions in 0.026Al steel during solidification process were calculated by Thermo-Calc software. As shown in Figure 6(a), the phase fraction of liquid gradually decreased with the decreasing of the temperature, i.e., the increasing of the solid fraction f_s of δ phase. When the temperature dropped to about 1701 K, γ phase emerged and the fraction of δ phase began to decrease. Besides, the contents of Al and N in liquid, δ, and γ
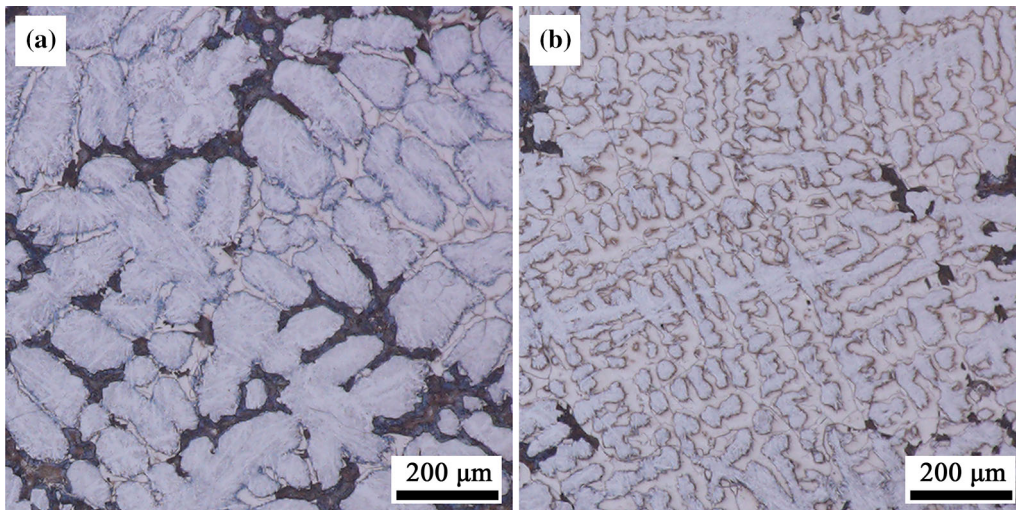

Fig. 4—The dendrite structure of the 0.026Al steel: (a) center; (b) edge.

phases are shown in Figure 6(b), which was used to calculate the equilibrium partition coefficients of Al and N ($k^{\delta/L}$ and $k^{\gamma/L}$) via Eq. [6].

The equilibrium partition coefficients of Al and N are shown in Figure 7(a). On the one hand, the equilibrium partition coefficients of Al were higher than 1, indicating that the consumption of Al in the residual liquid steel during solidification process, which was consistent with the study of Shen et al.[46] However, the equilibrium partition coefficients of N were lower than 1, revealing that the enrichment of N in the residual liquid steel, which was in agreement with the results of Shi et al.[25,47] On the other hand, when the temperature was lower than 1701 K, liquid, δ, and γ phases exist simultaneously. As for the three-phases coexistence zone, $k^{S/L}$ can be calculated from Eq. [13] according to the previous researches :[42,44,48,49]

$$k^{S/L} = m_\delta \cdot k^{\delta/L} + m_\gamma \cdot k^{\gamma/L} \quad [13]$$

$$m_\delta + m_\gamma = 1 \quad [14]$$

where $k^{\delta/L}$, $k^{\gamma/L}$, and $k^{S/L}$ are solute partition coefficients in the δ/L, γ/L and ($\delta+\gamma$)/L interface, respectively. m_δ and m_γ are the mass fractions of δ and γ phases in the solid phase, respectively. Hence, the equilibrium partition coefficients ($k^{S/L}$) of Al and N are shown in Figure 7(b). It can be seen that the values of $k^{\gamma/L}$ were closer to 1 than that of $k^{\delta/L}$, illustrating that the segregation degree of Al and N between γ and liquid phases was lower than that between δ and liquid phases. Therefore, taking N as an example, the values of $k^{\delta/L}$-N began to increase when γ phase emerged, i.e., the decreasing of the segregation degree of N between solid and liquid phases.

Figure 8(a) shows the diffusion coefficients of Al and N in δ and γ phases (D^δ and D^γ) calculated by DICTRA software. It can be seen that the diffusion coefficients of Al are far less than that of N. Similarly, the diffusion coefficients in the three-phase coexistence zone are calculated using Eq. [15] according to the previous researches:[42,44,48,49]

$$D^S = V_\delta \cdot D^\delta + V_\gamma \cdot D^\gamma \quad [15]$$

$$V_\delta + V_\gamma = 1 \quad [16]$$

where D^δ, D^γ, and D^S are diffusion coefficients in δ, γ, and $\delta+\gamma$ phases, respectively. V_δ and V_γ are the volume fractions of δ and γ phases in the solid phase, respectively. Accordingly, the diffusion coefficients of Al and N during solidification process are shown in
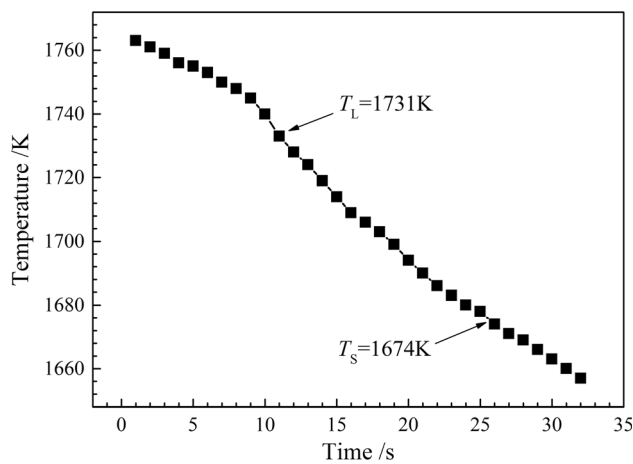

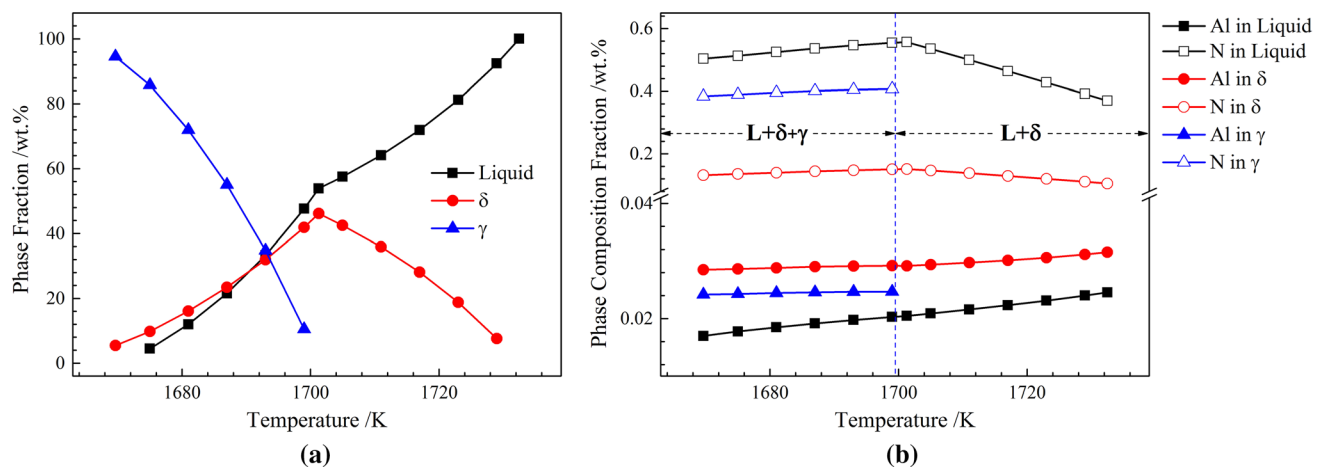Fig. 5—The cooling curve of the edge in experimental steel measured by the thermocouple.

Fig. 6—The equilibrium phase and phase composition fractions in 0.026Al steel during solidification process: (a) phase fractions; (b) phase composition fractions.
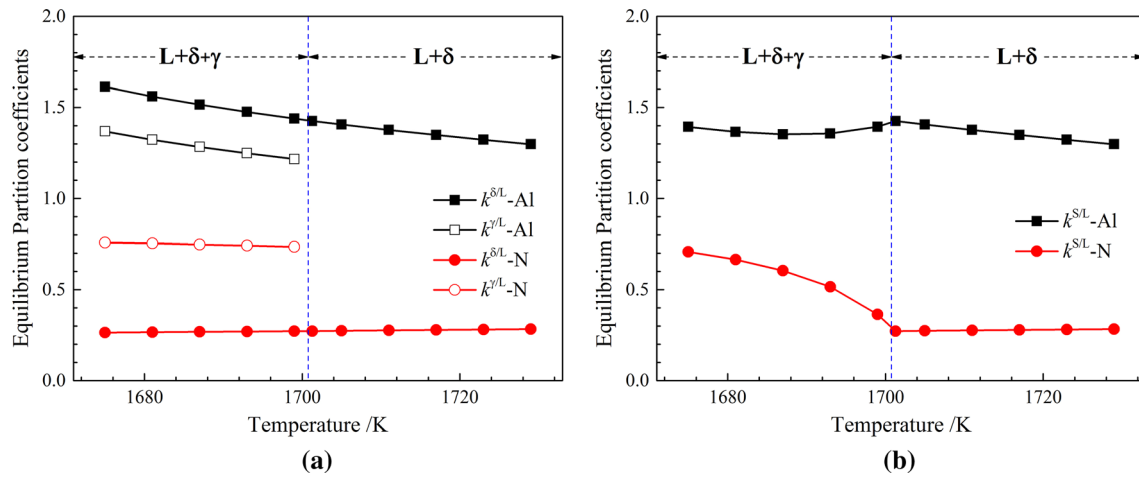
Fig. 7—The equilibrium partition coefficients of Al and N calculated by Thermo-Calc software: (a) $k^{\delta/L}$ and $k^{\gamma/L}$; (b) $k^{S/L}$.
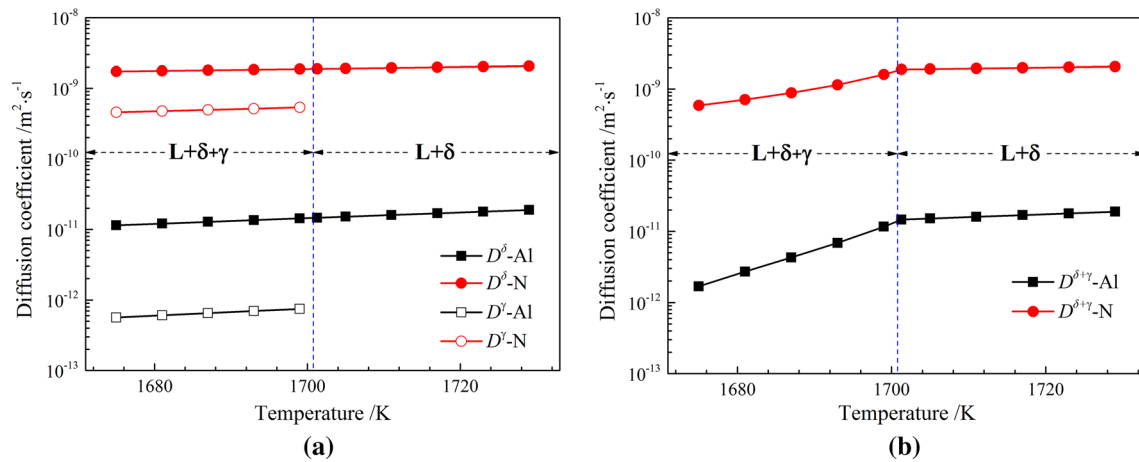

Fig. 8—The diffusion coefficients of Al and N calculated by DICTRA software: (a) D^{δ} and D^{γ}; (b) $D^{\delta+\gamma}$.

Figure 8(b). It is obvious that the diffusion coefficients of Al and N in δ phase were higher than those in γ phase. Consequently, the diffusion coefficients of Al and N in solid phase began to decrease when γ phase emerged.

According to Eqs. [5] through [16] and Figures 4 through 8, the variation of the concentrations of Al and N ([pct Al] and [pct N]) in the residual liquid steel during solidification process was calculated as shown in Figure 9. It could be seen that [pct Al] decreased with the increasing of solid fraction f_s, which corresponded to the equilibrium partition coefficients in Figure 7. [pct N] increased with the increasing of solid fraction f_s in the two-phase coexistence zone (liquid and δ phases). When γ phase emerged, [pct N] began to decrease. It is reported that the solubility of N in austenite was higher than that of ferrite,[4,23] thus N in the residual liquid would dissolve into the austenite matrix after the appearance of γ phase, resulting in the reduction of [pct N]. However, the concentrations of the solute elements in the center and edge of 0.026Al ingot were

basically the same, indicating that λ_S and C_R had little effect on the change of [pct Al] and [pct N] during solidification process.

Thereafter, the relationship between AlN formation and solid fraction in 0.026Al steel is shown in Figure 10. Here, Q_{AlN} is defined as the product of [pct Al] and [pct N] calculated by Figure 9. When the value of Q_{AlN} exceeded that of K_{AlN}^{prime} in Eq. [12], the thermodynamic condition of AlN formation would be reached. Taking concentrations of Al and N in the center as an example, it is obvious that the variation trend of Q_{AlN} (0.026Al) was basically consistent with [pct N] in Figure 9(b), illustrating that the change of [pct N] had more significant effect on Q_{AlN} (0.026Al). Furthermore, the value of Q_{AlN} (0.026Al) was lower than that of K_{AlN}^{prime} during the solidification process, revealing that AlN inclusion could not form. The variation of the Q_{AlN} in 0.045Al steel is also shown in Figure 10, and it could be seen that the value of Q_{AlN} (0.045Al) would exceed that of K_{AlN}^{prime} as f_S increased to 0.144. Hence, AlN inclusion
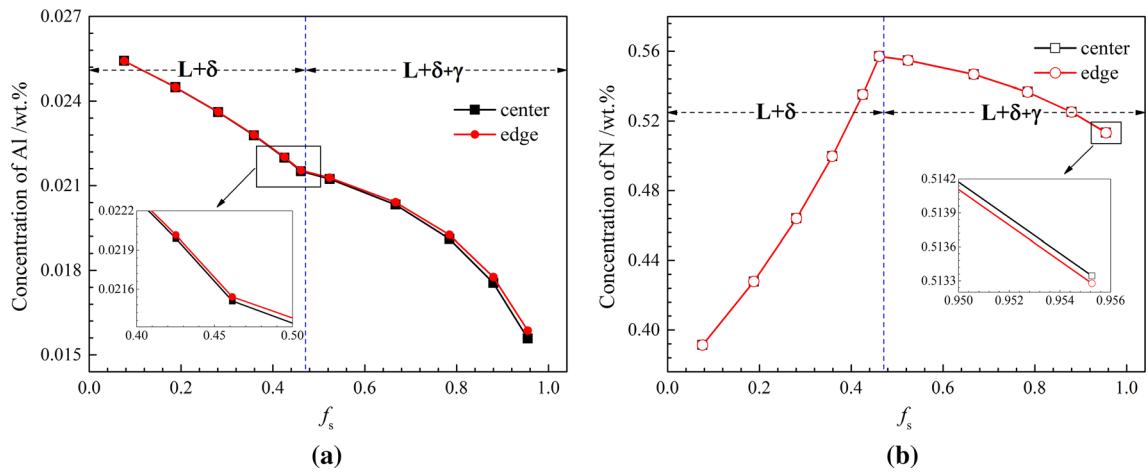
Fig. 9—The variation of the concentrations of Al and N in the residual liquid steel during solidification process: (*a*) [pct Al]; (*b*) [pct N].

could form in 0.045Al steel during the solidification process, which shows good agreement with morphology observation in Figure 2.

Obviously, the product of [pct Al] and [pct N] significantly varied as the proceeding of solidification process (the increasing of f_S) due to the segregation of Al and N in the residual liquid steel. Thus, the formation of AlN inclusion would occur when the concentration product of Al and N exceeded the critical solubility of AlN inclusion because of the enrichment of N. Based on the parameters of 0.026Al steel, the critical Al content of AlN formation when the N content is 0.40 wt pct during solidification process is approximately calculated as 0.030 wt pct, as shown in Figure 10. In other words, in order to prevent AlN formation during solidification process, the Al content in HNSBSs when the N content is 0.40 wt pct should be lower than 0.030 wt pct.

B. AlN Formation in HNSBSs during Heat Treatment Processes

It is obvious that the formation tendency of AlN in the liquid phase and during solidification process is little when the Al content is lower than 0.030 wt pct. Nevertheless, AlN inclusion could precipitate during heat treatment process because of the easy nucleation at high temperature.[50] Therefore, the formation mechanism of AlN precipitation during annealing (1023 K) and austenitizing (1323 K) processes was also investigated.

1. Characterization of AlN Inclusion in Annealed and Austenitized HNSBSs

Figure 11 shows the microstructure of 0.026Al steel annealed at 1023 K for 120 min and austenitized at 1323 K for 120 min. It can be seen that there was a large amount of Cr_2N precipitates in 0.026Al steel after annealing at 1023 K, as shown in Figure 11(a), and AlN inclusion was not found after careful examination. However, after austenitizing at 1323 K, AlN inclusion with the size of about 300 nm was detected (Figure 11(b)), while its size was much smaller than that in
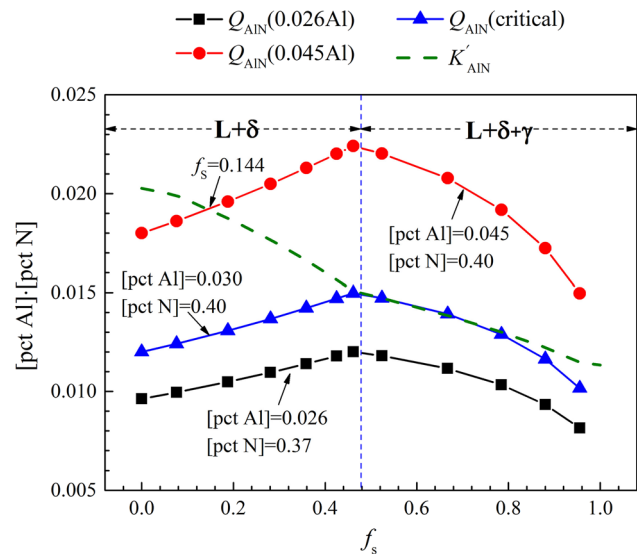

Fig. 10—The relationship between AlN formation and solid fraction in HNSBSs.

as-cast 0.076Al ingot. Accordingly, the precipitation tendency of AlN inclusion during austenitizing process was higher than that during annealing process.

Thereafter, the morphologies of inclusions in HNSBSs with various Al contents after austenitizing at 1323 K for 120 min were observed, and most inclusions were detected using EDS, as shown in Figure 12. It is obvious that no AlN inclusion was found in 0.006Al steel (Figure 12(a)), while AlN inclusion and a small amount of AlN-MnS composite inclusion appeared in the other five experimental steels (Figures 12(b) through (f)). In order to further confirm the type of inclusion, TEM examination was performed for 0.076Al steel, as shown in Figure 13. The inclusion exhibits rectangular shape, which is confirmed to be AlN with hexagonal close packed (hcp) structure based on the SAD pattern.
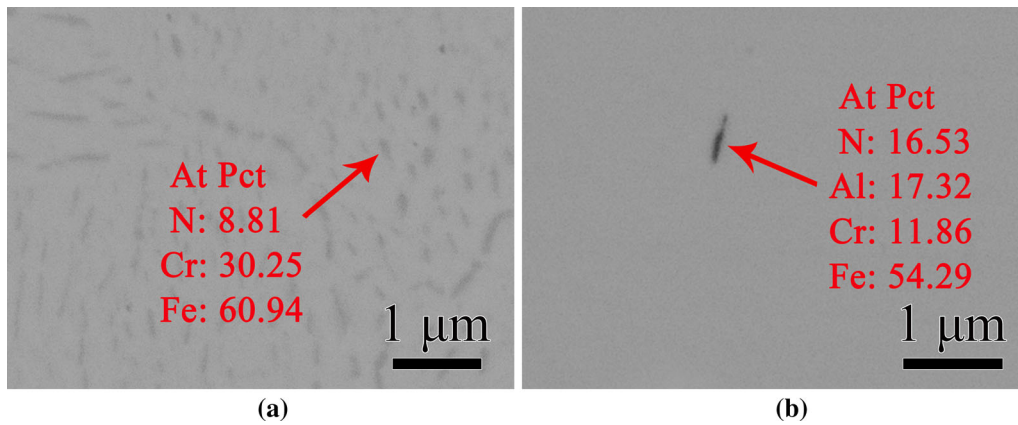
Fig. 11—The microstructure of 0.026Al steel (*a*) annealed at 1023 K and (*b*) austenitized at 1323 K for 120 min.
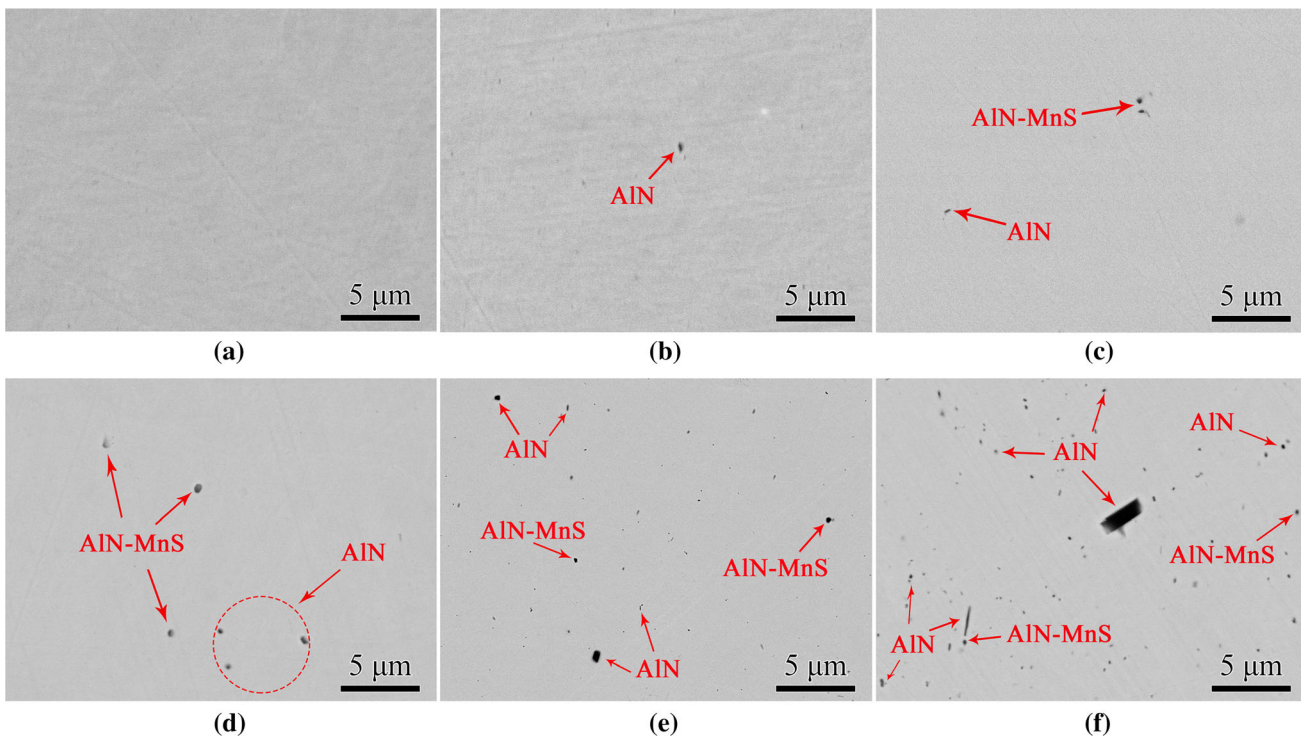

Fig. 12—The morphologies of inclusions in HNSBSs with various Al contents after austenitizing at 1323 K for 120 min: (*a*) 0.006Al; (*b*) 0.008Al; (*c*) 0.013Al; (*d*) 0.026Al; (*e*) 0.045Al, (*f*) 0.076Al.

The variation of the average size (*d*) and number density (N_A) of AlN inclusion is shown in Figure 14. On the one hand, all the AlN inclusions in 0.008Al steel were less than 0.5 μm, and the size of AlN inclusions in 0.013Al and 0.026Al steels was less than 0.6 μm. It is worth noting that the average size of AlN inclusions about 0.5 to 1.0 μm in 0.045Al and 0.076Al steels was larger than those with the Al content lower than 0.026 wt pct, and AlN inclusions about 1.0 to 5.0 μm emerged in 0.076Al steel, which formed in liquid steel and during solidification process according to the thermodynamic analysis above. Therefore, the larger AlN inclusions formed in liquid steel and during solidification process

would not dissolve during austenitizing process. On the other hand, the number density of AlN inclusion increased with the increasing of Al content from 0.008 wt pct to 0.076 wt pct. Especially for the inclusions with the size of 0.1 to 0.3 μm, the number density in 0.045Al and 0.076Al steels soared to 3.46×10^4 and 8.97×10^4 m^{-2}, respectively, which were dozens of times than those in other experimental steels. Kim *et al.*[50] also indicated the precipitation of small size AlN inclusion in the Al(N)-added medium C-Mn steels during reheating process because of a kinetically easy path for the nucleation of AlN. Consequently, the precipitation of

a large number of small size AlN inclusions in the experimental steels occurred during austenitizing process.

2. Thermodynamics and Kinetics Analysis of AlN Formation During Heat Treatment Process

According to the morphologies after heat treatment process in Figures 11 and 12, AlN inclusion could not precipitate in 0.026Al steel during annealing at 1023 K, while small size AlN inclusion emerged after austenitizing at 1323 K in HNSBSs with Al content higher than 0.006 wt pct. Therefore, in order to clarify the formation mechanism of AlN precipitation during heat treatment process, the thermodynamics and kinetics of AlN formation at different temperatures were analyzed.

In terms of thermodynamics, the Gibbs free energy change (ΔG) of AlN and Cr_2N in 0.026Al steel calculated by Thermo-Calc software is shown in Figure 15. It is obvious that the Gibbs free energy of Cr_2N at 1023 K (-6426.72 J mol^{-1}) is much lower than that at 1323 K

(-719.93 J mol^{-1}), revealing that Cr_2N is more sensitive to precipitate during annealing process, and the precipitation tendency of Cr_2N decreased significantly during austenitizing process. The Gibbs free energy of AlN at 1023 K (-310.12 J mol^{-1}) was close to that at 1323 K (-280.88 J mol^{-1}), while AlN inclusion was only detected at 1323 K. Accordingly, it could be inferred that the precipitation tendency of Cr_2N might affect the precipitation of AlN.

Meanwhile, the equilibrium phase fractions in HNSBSs calculated using Thermo-Calc software are shown in Figure 16. According to the equilibrium phase fractions of 0.026Al steel in Figure 16(a), AlN inclusion was stable either at 1023 K in α phase or at 1323 K in γ phase, while it only emerged after austenitizing at 1323 K. It is well known that the ferritic matrix exhibited very low N solubility.[7,23] During the annealing process at 1023 K, the precipitation of a large amount of Cr_2N (Figures 11(a) and 16(a)) consumed N in the matrix, thus the precipitation tendency of AlN was greatly
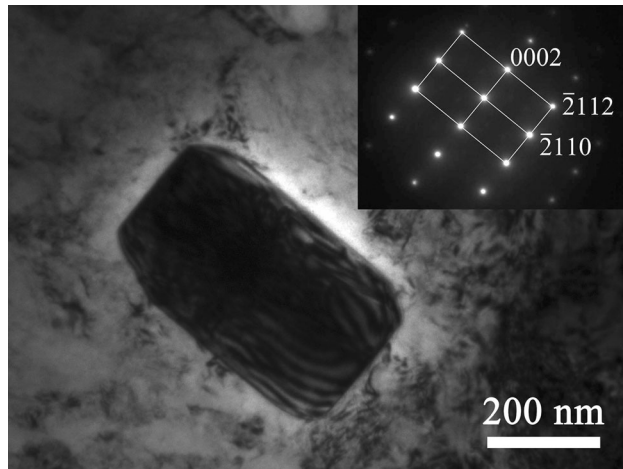

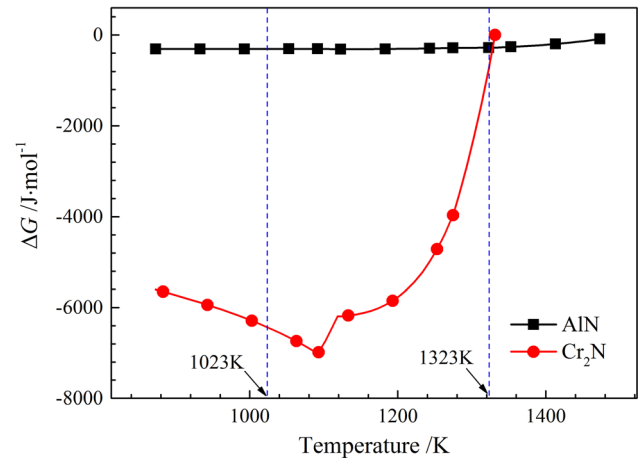Fig. 13—TEM micrograph and SAD patterns of 0.076Al steel.

Fig. 15—The Gibbs free energy change of AlN and Cr_2N in 0.026Al steel calculated by Thermo-Calc software.
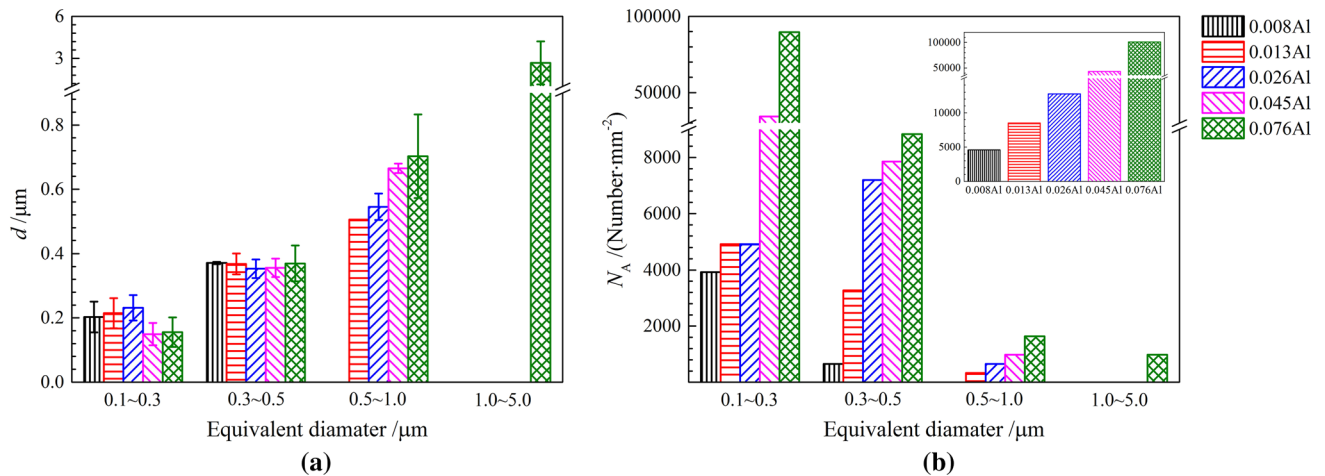

(a)

(b)

Fig. 14—The variation of the average size and number density of AlN inclusion in HNSBSs with various Al contents after austenitizing at 1323 K for 120 min: (a) average size d; (b) number density N_A.
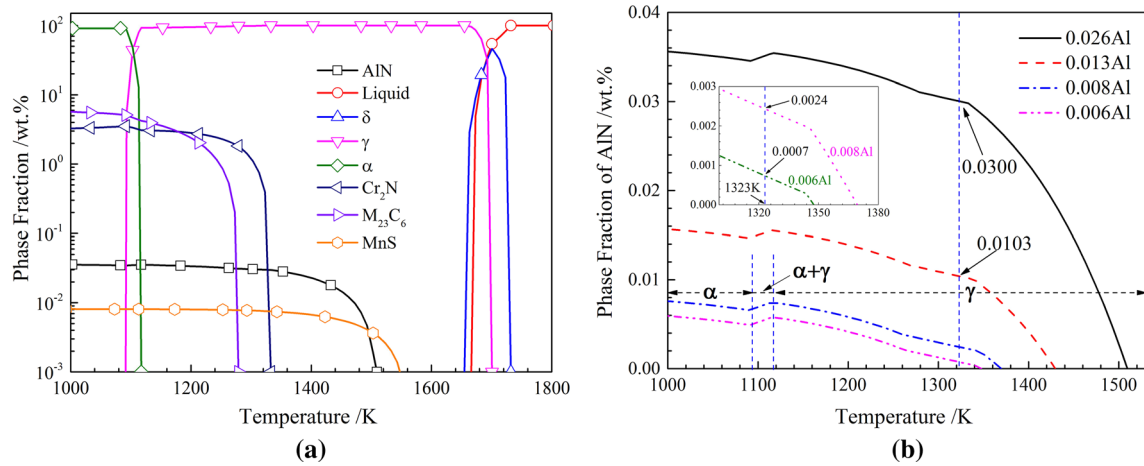
Fig. 16—The equilibrium phase fractions in HNSBSs calculated using Thermo-Calc software: (a) 0.026Al steel; (b) AlN equilibrium phase fractions.
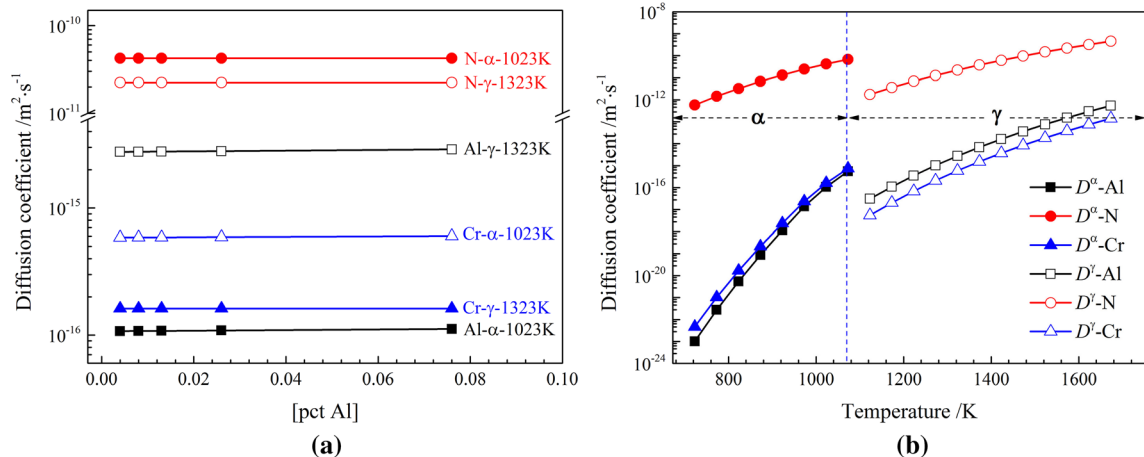

Fig. 17—The variation of diffusion coefficients of Al, N, and Cr in α and γ phases with (a) various Al contents and (b) temperatures.

reduced. Nevertheless, during austenitizing process at 1323 K, as shown in Figures 11(b) and 16(a), most Cr_2N precipitates could dissolve into γ phase; hence, AlN with higher stability was more likely to precipitate at 1323 K.

In terms of kinetics, the diffusion of Al and N also affected the formation of AlN in steels,[23] thus the diffusion coefficients of Al, N, and Cr in α and γ phases of HNSBSs were calculated using DICTRA software, in which the N content was set as 0.4 wt pct. Figure 17(a) shows the variation of diffusion coefficients of Al, N, and Cr in α and γ phases with various Al contents. It can be seen that the diffusion coefficients of Al, N, and Cr were basically unchanged as the Al content increased from 0.004 wt pct to 0.076 wt pct. Accordingly, taking 0.026Al steel as an example, the variation of diffusion coefficients of Al, N, and Cr in α and γ phases with temperature is shown in Figure 17(b). It is obvious that with the decreasing of temperature, the diffusion coefficients of Al and N in γ phase decreased, thus the

precipitation tendency of AlN decreased. Similarly, the diffusion coefficients of Al and N in α phase also decreased with the decreasing temperature. Simultaneously, the diffusion coefficient of Al is much lower than that of N in both the two phases. The diffusion coefficient values of N in α phase at 1023 K and in γ phase at 1323 K were 4.232×10^{-11} and 2.239×10^{-11} $m^2 \ s^{-1}$, respectively, which were in an order of magnitude. However, the diffusion coefficient value of Al in α phase at 1023 K was $1.074 \times 10^{-16} \ m^2 \ s^{-1}$, which was much lower than that in γ phase at 1323 K ($2.766 \times 10^{-15} \ m^2 \ s^{-1}$). In addition, the diffusion coefficient value of Al at 1323 K was higher than that of Cr ($5.872 \times 10^{-16} \ m^2 \ s^{-1}$), while the diffusion coefficient value of Al at 1023 K was lower than that of Cr ($1.621 \times 10^{-16} \ m^2 \ s^{-1}$), revealing that the interference degree of Cr on AlN precipitation during annealing process was higher than that during austenitizing process. Consequently, it can
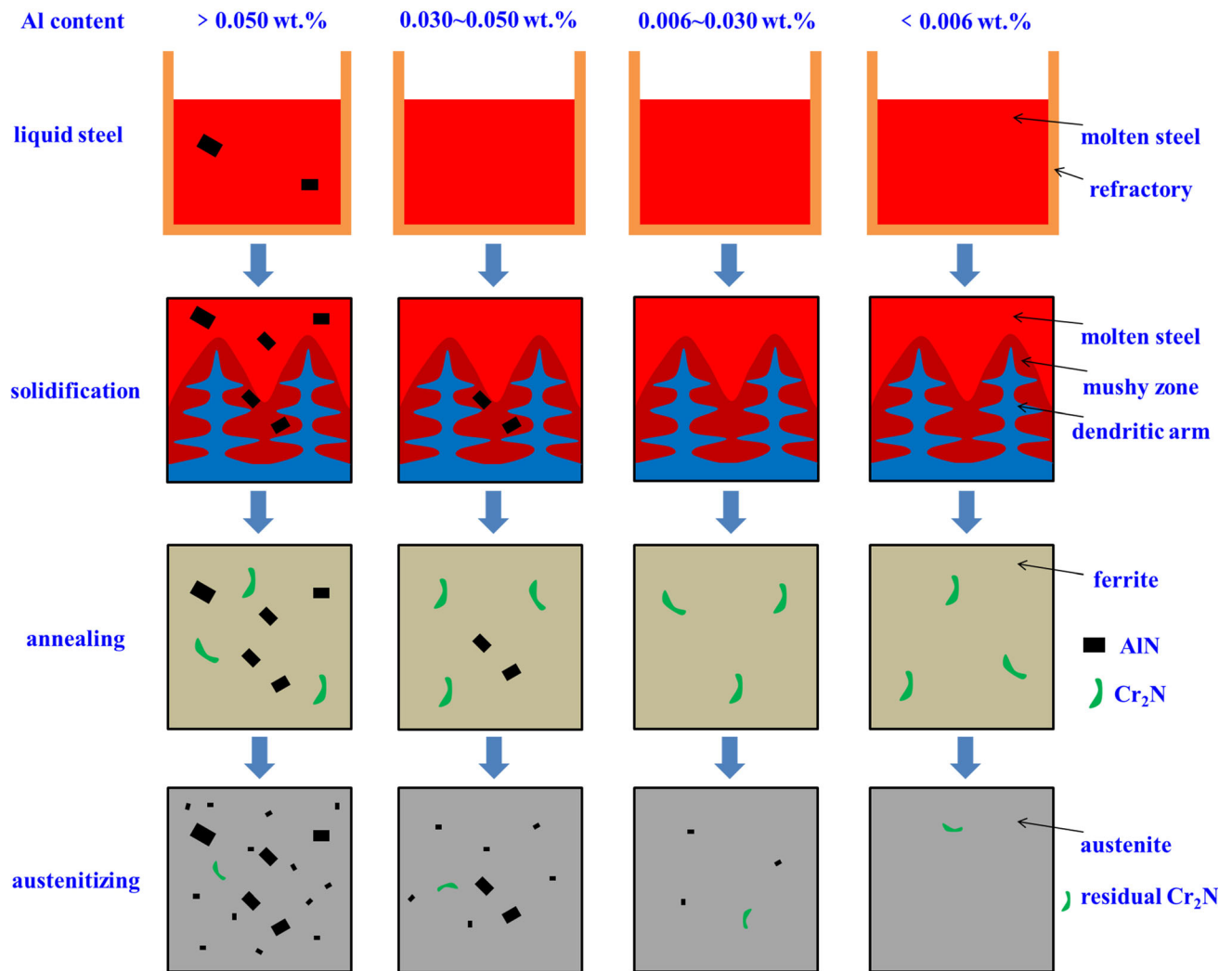
Fig. 18—The schematic illustration of the formation processes of AlN inclusion in HNSBSs with various Al contents.

be inferred that the extremely low diffusion coefficients of Al would also limit the precipitation of AlN at 1023 K, and AlN was more sensitive to precipitate at 1323 K.

In summary, during annealing process, the Gibbs free energy change of Cr_2N was much lower than that of AlN. The consumption of N in the matrix because of the precipitation of a large amount of Cr_2N, together with the extremely low diffusion coefficient of Al in α phase, made it hard to precipitate AlN during annealing process. Nevertheless, during austenitizing process, most Cr_2N precipitates could dissolve into γ phase, and the diffusion coefficients of Al were relatively high. Consequently, AlN was more sensitive to precipitate during austenitizing process, and some small size AlN inclusions emerged in HNSBSs.

Furthermore, as shown in Figure 16(b), it is obvious that the precipitation temperature and content of AlN inclusion at 1323 K decreased significantly with the decreasing of Al content. When the Al content dropped to 0.006 wt pct, the phase fraction of AlN inclusion in HNSBSs was only 0.0007 wt pct, which is much lower

than that in 0.008Al steel (0.0024 wt pct). Meanwhile, AlN inclusion could dissolve into the matrix at about 1348 K when the Al content was 0.006 wt pct. Combined with the morphologies in Figure 12, the phase fraction of AlN inclusion in 0.006Al steel was too low to precipitate AlN, thus AlN inclusions could precipitate during austenitizing process when the Al content was higher than 0.006 wt pct. Accordingly, it can be inferred that the critical Al content to avoid AlN precipitation in HNSBSs during austenitizing process is about 0.006 wt pct.

C. The Critical Al Content to Avoid AlN Formation in HNSBSs

As discussed above, the formation mechanism of AlN inclusion in HNSBSs under as-cast, annealing, and austenitizing states was different, and the formation processes of AlN inclusion were affected by the Al content. Therefore, in order to exhibit the critical Al content of AlN formation more clearly, the schematic

illustration of the formation processes of AlN inclusion in HNSBSs with various Al contents is shown in Figure 18.

When the Al content was higher than 0.050 wt pct, the product of [pct Al] and [pct N] could exceed the critical solubility of AlN inclusion in liquid steel, so AlN inclusions about 1 to 5 μm emerged in the molten steel. And then the thermodynamic conditions for AlN formation could also be satisfied during solidification process, hence AlN inclusions would form in the residual liquid steel. Furthermore, during annealing process, the precipitation of Cr_2N and the extremely low diffusion coefficient of Al in α phase restrained the precipitation of AlN, so there was no further formation of AlN inclusion. However, during austenitizing process, most Cr_2N precipitates dissolved into γ phase, and the diffusion coefficients of Al were higher than that in annealing process, which increased the precipitation tendency of AlN. Consequently, a large amount of small size AlN inclusions precipitated in austenite matrix due to its easy nucleation at high temperature. It is worth emphasizing that large size AlN in as-cast HNSBSs formed in liquid steel and during solidification process would remain during heat treatment processes.

Subsequently, when the Al content was between 0.030 wt pct and 0.050 wt pct, the thermodynamic conditions for AlN formation could not be satisfied in liquid steel, i.e., AlN inclusion could not form. Nevertheless, during solidification process, AlN inclusion would form in the residual liquid steel when the concentration product of Al and N exceeded the critical solubility of AlN inclusion due to the enrichment of N. Accordingly, some AlN inclusions formed at the solidifying front in the mushy zone. Subsequently, the formation processes of AlN inclusion during heat treatment processes were similar to that in HNSBSs with Al content higher than 0.050 wt pct.

Moreover, when the Al content was between 0.006 and 0.030 wt pct, the thermodynamic conditions for AlN formation in liquid steel or during solidification process could not be satisfied. Hence, AlN inclusion could not form in as-cast HNSBSs, while only a few small size AlN inclusions could precipitate during austenitizing process.

Finally, as the Al content decreased to 0.006 wt pct, AlN inclusion was also not detected in the austenitized samples. Consequently, when the Al content was lower than 0.006 wt pct, AlN inclusion would not form in HNSBSs after melting, solidification, and heat treatment processes.

IV. CONCLUSIONS

In the present study, the formation mechanism of AlN inclusion in high-nitrogen stainless bearing steels was systematically studied, and the main conclusions are as follows:

1. The concentration product of Al and N could exceed the critical solubility of AlN inclusion at liquidus temperature when the Al content was higher than 0.050 wt pct; thus, AlN inclusions (about 1 to 5 μm) could form in liquid HNSBSs.
2. According to the calculations on 'Clyne-Kurz' model, AlN inclusion could form during solidification process because of the enrichment of N in the residual liquid steel with the Al content higher than 0.030 wt pct.
3. The precipitation of Cr_2N and the extremely low diffusion coefficient of Al in α phase restrained the precipitation of AlN during annealing process. AlN and AlN-MnS composite inclusions less than 0.6 μm could precipitate due to its easy nucleation during austenitizing process.

Combined with morphology observation and thermodynamic, kinetic analysis, the critical Al content to avoid AlN formation in HNSBSs after melting, solidification, and heat treatment processes is 0.006 wt pct.

REFERENCES

1. J. Dai, H. Feng, H.B. Li, Z.H. Jiang, H. Li, S.C. Zhang, P. Zhou, and T. Zhang: *Corros. Sci.*, 2020, vol. 174, art. no. 108792.
2. H.B. Li, Z.H. Jiang, H. Feng, S.C. Zhang, L. Li, P.D. Han, R.D.K. Misra, and J.Z. Li: *Mater. Des.*, 2015, vol. 84, pp. 291–99.
3. D.W. Kim: *J. Nucl. Mater.*, 2012, vol. 420, pp. 473–78.
4. W. Horvath, W. Prantl, H. Stroißnigg, and E.A. Werner: *Mater. Sci. Eng. A*, 1998, vol. 256, pp. 227–36.
5. C.O.A. Olsson: *Corros. Sci.*, 1995, vol. 37, pp. 467–79.
6. G. Lothongkum, P. Wongpanya, S. Morito, T. Furuhara, and T. Maki: *Corros. Sci.*, 2006, vol. 48, pp. 137–53.
7. H. Feng, Z.H. Jiang, H.B. Li, P.C. Lu, S.C. Zhang, H.C. Zhu, B.B. Zhang, T. Zhang, D.K. Xu, and Z.G. Chen: *Corros. Sci.*, 2018, vol. 144, pp. 288–300.
8. H. Feng, H.B. Li, Z.H. Jiang, T. Zhang, N. Dong, S.C. Zhang, P.D. Han, S. Zhao, and Z.G. Chen: *Corros. Sci.*, 2019, vol. 158, art. no. 108081.
9. V. Valasamudram, S.T. Selvamani, M. Vigneshwar, V. Balasubramanian, and D. Jayaperumal: *Mater. Today: Proc.*, 2018, vol. 5, pp. 8338–47.
10. W.C. Jiao, H.B. Li, J. Dai, H. Feng, Z.H. Jiang, T. Zhang, D.K. Xu, H.C. Zhu, and S.C. Zhang: *J. Mater. Sci. Technol.*, 2019, vol. 35, pp. 2357–64.
11. W. Trojahn, E. Streit, H.A. Chin, and D. Ehlert: *Materialwiss. Werkstofftech.*, 1999, vol. 30, pp. 605–11.
12. Z.X. Cao, Z.Y. Shi, B. Liang, X.D. Zhang, W.Q. Cao, and Y.Q. Weng: *Int. J. Fatigue*, 2020, vol. 140, art. no. 105854.
13. Z.K. Li, J.Z. Lei, H.F. Xu, F. Yu, H. Dong, and W.Q. Cao: *J. Iron Steel Res. Int.*, 2016, vol. 28, pp. 1–12.
14. Q.R. Tian, G.C. Wang, Y. Zhao, J. Li, and Q. Wang: *Metall. Mater. Trans. B*, 2018, vol. 49B, pp. 1149–64.

15. Z.X. Cao, Z.Y. Shi, F. Yu, G.L. Wu, W.Q. Cao, and Y.Q. Weng: *Int. J. Fatigue*, 2019, vol. 126, pp. 1–5.
16. C.Y. Yang, P. Liu, Y.K. Luan, D.Z. Li, and Y.Y. Li: *Int. J. Fatigue*, 2019, vol. 128, art. no. 105193.
17. Y.G. Chi, Z.Y. Deng, and M.Y. Zhu: *Metall. Mater. Trans. B*, 2018, vol. 49, pp. 440–50.
18. J. Jang, M. Paek, and J. Pak: *ISIJ Int.*, 2017, vol. 57, pp. 1821–30.
19. L.W. Xu, H.B. Li, H.B. Zheng, P.C. Lu, H. Feng, S.C. Zhang, W.C. Jiao, and Z.H. Jiang: *J. Iron Steel Res. Int.*, 2020, vol. 27, pp. 1466–75.
20. Z.W. Hou, M. Jiang, E.J. Yang, S.Y. Gao, and X.H. Wang: *Metall. Mater. Trans. B*, 2018, vol. 49B, pp. 3056–66.
21. J.H. Park and Y. Kang: *Steel Res. Int.*, 2017, vol. 88, p. 1700130.
22. C.L. Zheng, B. Lv, F.C. Zhang, Z.N. Yang, J. Kang, L. She, and T.S. Wang: *Scr. Mater.*, 2016, vol. 114, pp. 13–16.
23. F.G. Wilson and T. Gladman: *Int. Mater. Rev.*, 1988, vol. 33, pp. 221–86.
24. N.H. Croft, A.R. Entwisle, and G.J. Davies: *Metals Technol.*, 2013, vol. 10, pp. 125–29.
25. C.B. Shi, X.C. Chen, and H.J. Guo: *Int. J. Miner. Metall. Mater.*, 2012, vol. 19, pp. 295–302.
26. H. Liu, J. Liu, S. Michelic, F. Wei, C. Zhuang, Z. Han, and S. Li: *Ironmak. Steelmak.*, 2015, vol. 43, pp. 1–9.
27. R. Rene, S. Sabine, Z. Sabine, and K. Ernst: *Steel Res. Int.*, 2011, vol. 82, pp. 905–10.
28. R. Radis and E. Kozeschnik: *Modell. Simul. Mater. Sci. Eng.*, 2010, vol. 18, art. no. 055003.
29. L.M. Cheng, E.B. Hawbolt, and T.R. Meadowcroft: *Scr. Mater.*, 1999, vol. 41, pp. 673–78.
30. M. Lückl, T. Wojcik, E. Povoden-Karadeniz, S. Zamberger, and E. Kozeschnik: *Steel Res. Int.*, 2017, vol. 89, p. 1700342.
31. Y. Luo, M. Li, P.R. Scheller, S. Sridhar, and L.F. Zhang: *Metall. Mater. Trans. B*, 2019, vol. 50B, pp. 2459–70.
32. J. Bott, H.B. Yin, and S. Sridhar: *Metall. Mater. Trans. B*, 2014, vol. 45B, pp. 2222–31.
33. Y.L. Chen, Y. Wang, and A.M. Zhao: *J. Iron Steel Res. Int.*, 2012, vol. 19, pp. 51–56.
34. H. Feng, H.B. Li, X.L. Wu, Z.H. Jiang, S. Zhao, T. Zhang, D.K. Xu, S.C. Zhang, H.C. Zhu, B.B. Zhang, and M.X. Yang: *J. Mater. Sci. Technol.*, 2018, vol. 34, pp. 1781–90.
35. H. Wada and R.D. Pehlke: *Metall. Trans. B*, 1979, vol. 10B, pp. 409–12.
36. G. Sigworth and J. Elliott: *Met. Sci.*, 1974, vol. 8, pp. 298–310.
37. S.B. Lee, D. Kim, and J.J. Pak: *ISIJ Int.*, 2009, vol. 49, pp. 337–42.
38. D.H. Kim, M.S. Jung, H. Nam, M.K. Paek, and J.J. Pak: *Metall. Mater. Trans. B*, 2012, vol. 43B, pp. 1106–12.
39. H. Ohta and H. Suito: *Metall. Mater. Trans. B*, 1996, vol. 27B, pp. 943–53.
40. S.K. Choudhary and A. Ghosh: *ISIJ Int.*, 2009, vol. 49, pp. 1819–27.
41. M. Paek, J. Jang, M. Jiang, and J. Pak: *ISIJ Int.*, 2013, vol. 53, pp. 973–78.
42. L.T. Gui, M.J. Long, Y.W. Huang, D.F. Chen, H.B. Chen, H.M. Duan, and S. Yu: *Metall. Mater. Trans. B*, 2018, vol. 49B, pp. 3280–92.
43. J.H. Shin and J.H. Park: *Metall. Mater. Trans. B*, 2020, vol. 51B, pp. 1211–24.
44. Y.W. Huang, M.J. Long, P. Liu, D.F. Chen, H.B. Chen, L.T. Gui, T. Liu, and S. Yu: *Metall. Mater. Trans. B*, 2017, vol. 48B, pp. 2504–15.
45. H.C. Zhu, Z.H. Jiang, H.B. Li, J.H. Zhu, H. Feng, S.C. Zhang, B.B. Zhang, P.B. Wang, and G.H. Liu: *Steel Res. Int.*, 2017, vol. 88, p. 1600509.
46. Y.Z. Shen, J.H. Liu, H. Xu, and H.B. Liu: *Metall. Mater. Trans. B*, 2020, vol. 51B, pp. 2963–75.
47. F. Yang, W.C. Zhao, Y. Hou, X.L. Guo, Q. Li, X. Li, J.B. Yu, Y.B. Zhong, K. Deng, and Z.M. Ren: *ISIJ Int.*, 2020, vol. 61, pp. 229–38.
48. L. Gui, M. Long, D. Chen, J. Zhao, Q. Wang, and H. Duan: *J. Mater. Res. Technol.*, 2020, vol. 9, pp. 89–103.
49. Y. Ueshima, S. Mizoguchi, T. Matsumiya, and H. Kajioka: *Metall. Trans. B*, 1986, vol. 17B, pp. 845–59.
50. J.M. Kim and J.K. Park: *Philos. Mag. Lett.*, 2017, vol. 97, pp. 1–8.